

Low-Rank Adaptation of Neural Fields

ANH TRUONG, Massachusetts Institute of Technology, USA

AHMED H. MAHMOUD, Massachusetts Institute of Technology, USA

MINA KONAKOVIĆ LUKOVIĆ, Massachusetts Institute of Technology, USA

JUSTIN SOLOMON, Massachusetts Institute of Technology, USA

Processing visual data often involves small adjustments or sequences of changes, e.g., image filtering, surface smoothing, and animation. While established graphics techniques like normal mapping and video compression exploit redundancy to encode such small changes efficiently, the problem of encoding small changes to neural fields—neural network parameterizations of visual or physical functions—has received less attention. We propose a parameter-efficient strategy for updating neural fields using low-rank adaptations (LoRA). LoRA, a method from the parameter-efficient fine-tuning LLM community, encodes small updates to pre-trained models with minimal computational overhead. We adapt LoRA for instance-specific neural fields, avoiding the need for large pre-trained models and yielding lightweight updates. We validate our approach with experiments in image filtering, geometry editing, video compression, and energy-based editing, demonstrating its effectiveness and versatility for representing neural field updates.

CCS Concepts: • **Computing methodologies** → **Computer graphics**; **Machine learning**.

Additional Key Words and Phrases: LoRA, Neural Fields, Parameter-Efficient Fine-Tuning, Compression, SDF, Energy Minimization

ACM Reference Format:

Anh Truong, Ahmed H. Mahmoud, Mina Konaković Luković, and Justin Solomon. 2025. Low-Rank Adaptation of Neural Fields. In *SIGGRAPH Asia 2025 Conference Papers (SA Conference Papers '25)*, December 15–18, 2025, Hong Kong, Hong Kong. ACM, New York, NY, USA, 11 pages. <https://doi.org/10.1145/3757377.3763882>

1 Introduction

Processing visual data often involves small adjustments or sequences of changes. For example, image filtering usually involves local operations that alter the appearance but preserve the overall structure of an input image. Similarly, local surface edits—such as smoothing or sharpening—produce perturbative displacements from the original surface. Finally, videos consist of image frames where the difference between any two consecutive frames is likely small.

It should be possible to store small changes compactly. Built on this observation, classical methods in graphics reduce redundancy for different representations by only storing what is necessary to



Fig. 1. We encode diverse types of variations—including (from left to right) surface deformations, image changes, energy-based denoising, videos, and physical simulation—as compact low-rank updates to pre-trained neural fields. Despite operating with $7 - 8\times$ fewer parameters than for full fine-tuning, our approach achieves visually faithful reconstructions across a range of tasks.

realize a change. For instance, normal maps store surface displacements as compact textures encoding bumps and dents [Cook 1984]. Similarly, video codecs reduce temporal redundancy by using intermediate P-frames that store offsets from previous frames [Beach and Owen 2018]. In contrast, methods for compactly perturbing neural fields—an emerging representation in graphics and vision—have received little attention.

Neural fields represent physical or visual quantities (e.g., distances, density, color) in the weights of neural networks [Takikawa et al. 2023b]. Neural fields have desirable properties (e.g., continuity, differentiability, compact size, and ease of querying) that make them attractive for visual computing applications like deformation [Mehta et al. 2022], elastic simulation [Modi et al. 2024], and image processing [Luzi et al. 2024]. Like the classical examples above, many of these tasks yield small updates to a pre-trained model.

Editing a neural field, however, is far from straightforward, as there is a highly non-linear relationship between changes in its weights and the resulting changes in the output. Many specialized methods have been proposed to edit specific classes of neural fields (e.g., NeRFs [Liu et al. 2021] and neural SDFs [Wang et al. 2021]) but require large memory footprints and/or elaborate training pipelines, e.g., involving full fine-tuning or auxiliary networks.

In this paper, we present a parameter-efficient strategy for updating neural fields to capture small changes in an input function using low-rank adaptations (LoRA) [Hu et al. 2022]. LoRA is a popular method in the large language model (LLM) community for parameter-efficient fine-tuning of pre-trained networks to adapt to minor distributional shifts.

Authors' Contact Information: Anh Truong, Department of Electrical Engineering and Computer Science, Massachusetts Institute of Technology, Cambridge, MA, USA, anh_t@mit.edu; Ahmed H. Mahmoud, Computer Science & Artificial Intelligence Laboratory, Massachusetts Institute of Technology, Cambridge, MA, USA, ahdhn@mit.edu; Mina Konaković Luković, Department of Electrical Engineering and Computer Science, Massachusetts Institute of Technology, Cambridge, MA, USA, minakl@mit.edu; Justin Solomon, Department of Electrical Engineering and Computer Science, Massachusetts Institute of Technology, Cambridge, MA, USA, jsolomon@mit.edu.

SA Conference Papers '25, Hong Kong, Hong Kong

© 2025 Copyright held by the owner/author(s). Publication rights licensed to ACM. This is the author's version of the work. It is posted here for your personal use. Not for redistribution. The definitive Version of Record was published in *SIGGRAPH Asia 2025 Conference Papers (SA Conference Papers '25)*, December 15–18, 2025, Hong Kong, Hong Kong, <https://doi.org/10.1145/3757377.3763882>.

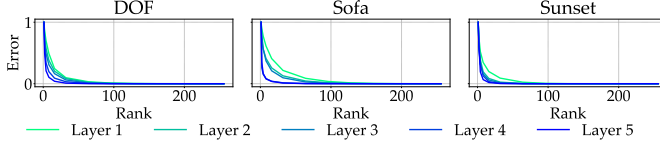


Fig. 2. Low-rank weight approximation error across layers of three fine-tuned image neural fields. A minor edit is performed to the target image of each neural field, and each neural field is fine-tuned to overfit to its edited image. The vertical axis measures the (normalized) approximation error of a rank-constrained factorization of the weight difference, accounting for the input distribution of the layer. A low rank approximation is sufficient to recover the fully fine-tuned weight with minimal error.

Our key insight is that typical updates to the function represented by a neural field—e.g., filtering or other local modifications—correspond to small shifts in the underlying data distribution. This makes strategies from parameter-efficient fine-tuning relevant. In particular, we observe that the *low-rank* structure imposed by LoRA provides a natural parameterization for such updates. As a motivating experiment, we fine-tuned image neural fields with weights W_{base} to match minor variations in their target images, resulting in updated weights $W_{\text{fine-tuned}}$. We found that a **low-rank factorization of the weight difference $W_{\text{fine-tuned}} - W_{\text{base}}$ approximates the true update with little error** when accounting for the layer’s input distribution (see Figure 2 and the Supplemental Material). Rather than computing this low-rank difference post hoc via full fine-tuning, LoRA allows us to *directly* learn the low-rank update. This makes it a principled and lightweight tool for neural field editing.

Unlike prior LoRA applications in visual computing (e.g., style transfer [Liu et al. 2024; Shah et al. 2025]) which fine-tune large, pre-trained models on datasets containing numerous examples, we apply LoRA to *instance-specific* neural fields. These are small networks overfit to individual signals (e.g., an image or an SDF). This setting avoids reliance on large pre-trained models and better suits common editing tasks in graphics.

We demonstrate the versatility of LoRAs for neural field updates with experiments in image, SDF, video, and energy minimization applications. Our experiments show that our method can effectively adapt pre-trained neural fields to faithfully encode edits while using **7-8× fewer parameters than conventional fine-tuning** (see Figure 3).

In summary, our contributions are:¹

- A parameter-efficient strategy for perturbing a neural field using LoRA.
- Experimental validation demonstrating the effectiveness and versatility of LoRA for neural field updates across a range of applications, including image filtering, geometry editing, video compression, and energy minimization (Figure 1).

While time-efficient model adaptation is a growing research area, the empirical benefits presented in this work focus on storage efficiency.

¹Code is available at <https://github.com/dinhhanhtruong/LoRA-NF>.

We begin by reviewing related work in §2 and introducing the preliminaries of neural fields in §3. We then present our LoRA-based strategy for updating generic neural fields in §4, describe its implementation for specific field types in §5, and conclude with our experimental findings in §7.

2 Related Work

2.1 Neural Fields

Neural fields are coordinate-based neural networks that serve as a flexible representation for data in visual computing (see survey by Takikawa et al. [2023b]). By parameterizing spatially- and time-varying physical properties of scenes or objects which lack closed-form expressions, neural fields support a wide range of applications, e.g., surface modeling [Park et al. 2019], scene reconstruction [Mescheder et al. 2019], inverse rendering [Mildenhall et al. 2021], signal processing [Sitzmann et al. 2020], and physics-informed simulation [Raissi et al. 2019]. Their desirable properties—continuity, full differentiability, and independence from spatial discretization—make them attractive for these tasks.

Neural fields are typically trained either to overfit a single instance (e.g., an image or SDF) or to generalize across a collection of instances using shared weights and instance-specific latent codes [Park et al. 2019]. The former—instance-specific neural fields—are increasingly used as a primary representation of graphics data [Davies et al. 2021], as they permit dedicating the full capacity of the network to a single signal. Once trained, these models can serve as drop-in replacements for the data they encode—e.g., a neural SDF can be used for downstream geometry processing tasks such as fast closest-point queries [Sharp and Jacobson 2022] or Constructive Solid Geometry operations upon minor refinement [Marschner et al. 2023]. Compared to traditional graphics representations, instance-specific neural fields are often more memory-efficient.

To further compress neural fields, various methods target the network weights themselves. Techniques such as weight quantization, model pruning [Chen et al. 2021], and low-rank tensor factorizations [Chen et al. 2022] have been proposed for lossy compression of network parameters. We focus on this instance-specific setting.

Most neural fields are parameterized using multi-layer perceptrons (MLPs), leveraging the universal approximation theorem [Kim and Adalı 2003]. To accelerate training and improve fidelity, MLPs are frequently augmented with auxiliary data structures, e.g., grids of latent vectors [Martel et al. 2021; Müller et al. 2022] or sparse hierarchical encodings [Takikawa et al. 2021]. While these hybrid architectures often improve convergence and quality [Takikawa et al. 2023a], they can introduce implementation complexity and increase memory usage at inference time, especially at high resolutions. For simplicity and broad compatibility, we restrict our method to standard MLP-based neural fields without auxiliary parameters.

2.2 Neural Field Editing

Editing a neural field to fit observed data or minimize energy functionals is not straightforward, as there is a highly non-linear relationship between changes in the weights of the network and the resulting changes in the network output. Recent works have proposed neural field editing techniques which fall under three broad

categories [Takikawa et al. 2023b]: (1) network fine-tuning where parameters of a pre-trained neural field are further optimized to fit edited data observations [Liu et al. 2021] or conform to energy terms [Marschner et al. 2023]; (2) using hypernetworks trained to map data distributions to neural field parameters [Chiang et al. 2022]; (3) latent code fine-tuning/interpolation for networks conditioned on latent codes [Hao et al. 2020]. Our investigation focuses on network fine-tuning, because hypernetworks require access to a data distribution which may be unavailable and unwanted for performing simple edits, and latent-code models are outside the scope of this work (see §2.1).

Closest to our approach, prior works in neural field fine-tuning have explored applying updates to a subset of a pre-trained neural field’s parameters. Liu et al. [2021] propose fine-tuning later layers of a pre-trained NeRF jointly with their latent codes. Their hybrid approach allows them to avoid the cost of fully tuning the network, but earlier layers remain fixed, limiting the expressivity of the network update. Mazzucchelli et al. [2024] observe that neurons in the final layer of a NeRF’s color MLP encode either view-dependent or diffuse appearance. By selectively fine-tuning only the neurons associated with diffuse appearance, their method is able to quickly re-color NeRF scenes. Similarly, Lee and Kim [2023] analyze neuron activations to select and fine-tune only those that contribute the most to the color of specific spatial regions. Recently, Kang et al. [2025] apply low-rank updates to factorized tri-plane features, which are aggregated and used as input to a fine-tuned MLP. These methods, however, assume that the pre-trained model has a specific NeRF architecture and/or that only a specific attribute (e.g. color) is to be edited.

2.3 Low-Rank Adaptations

LoRA [Hu et al. 2022] is a widely-used strategy for parameter-efficient fine-tuning of foundation models such as LLMs. By imposing a low-rank constraint on model weight updates, LoRA is effective at adapting pre-trained models to downstream tasks with few additional parameters. Beyond their original setting in LLM fine-tuning, LoRAs have been applied to other foundation models, predominantly diffusion models for image, video, and 3D data [Dagli et al. 2024; Lu et al. 2024; Ouyang et al. 2024] in tasks such as stylization [Liu et al. 2024; Wang et al. 2022], text-based editing [Qi et al. 2024; Zhao et al. 2024], and generative modeling [Wang et al. 2024].

While prior works demonstrate impressive task adaptation using LoRA, they typically operate in settings where large-scale pre-trained models are available, e.g., LLMs or diffusion models. These models contain billions of parameters and are often the result of costly and resource-intensive training pipelines. In contrast, our setting focuses on direct adaptation of instance-specific neural fields where no such large-scale pre-training is involved.

3 Preliminaries

Here, we establish notation used in the rest of the paper. We define a neural field as a continuous function $f_\theta : \mathbb{R}^m \rightarrow \mathbb{R}^n$ parameterized by the weights θ of a neural network, mapping spatial coordinates to values. The input/output dimensions m and n depend on the target signal. For example, a SDF has $m = 3$, $n = 1$ and maps 3D

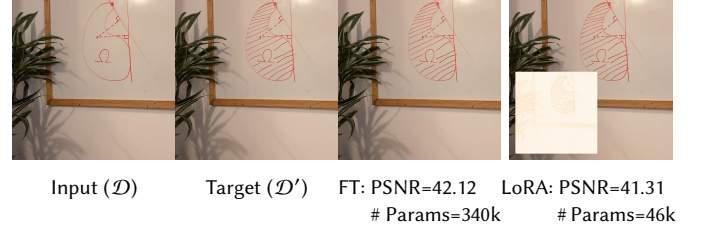


Fig. 3. Comparison between full fine-tuning (FT) and our LoRA-based approach for adapting a neural field to an image variation. The original image \mathcal{D} is edited to produce \mathcal{D}' by adding red marker strokes. LoRA reconstructs the edited image with high fidelity achieving a PSNR of 41.31 vs. 42.12 for FT while using $\approx 7.4\times$ fewer parameters (46k vs. 340k). The inset shows the difference image between LoRA and FT outputs.

coordinates to signed distances, while an RGB image has $m = 2$, $n = 3$ and maps 2D coordinates to RGB values. Throughout this work, we assume f_θ is overfit to a *single* instance of graphics data (e.g., one image or shape) by minimizing the reconstruction error between the neural field output and target signal.

We adopt the most basic neural field architecture: a multi-layer perceptron (MLP) that maps spatial coordinates to field values. An MLP consists of alternating linear layers and elementwise nonlinearities, e.g., ReLU. Following prior work [Mildenhall et al. 2021; Müller et al. 2022], we first apply a frequency (positional) encoding γ to the input coordinates before feeding them to the MLP:

$$\gamma(x) := (\sin(2^0 x), \cos(2^0 x), \dots, \sin(2^{L-1} x), \cos(2^{L-1} x)),$$

where $L \in \mathbb{N}$. Frequency encodings have proven effective in helping MLPs to regress high-frequency content. Composing the steps of our construction, we therefore consider neural fields of the form $f_\theta(x) := \text{MLP}_\theta(\gamma(x))$.

4 Low-rank Adaptation of Neural Fields

The input to our method consists of (1) a neural field f_θ representing a single graphics instance \mathcal{D} (e.g., an image or a SDF) and (2) an edited variant \mathcal{D}' of \mathcal{D} , which can either be explicitly provided (§5.1, §5.2) or implicitly characterized, e.g., as the solution of an energy minimization problem (§5.3). In the latter case, the corresponding energy functional characterizing \mathcal{D}' is taken as input.

Our method outputs a set of additive weight updates to f_θ as low-rank adapters, defined below. When these updates are applied to f_θ , they approximate the edited instance \mathcal{D}' . This approach encodes the edit made to \mathcal{D} as a low-rank update to the base neural field f_θ . We also explore an extension of this setup for *sequences* of edits (§5.4).

As discussed in §2, existing methods primarily update neural fields by directly fine-tuning the network on new training objectives. This approach typically involves either storing a full copy of the base model weights or discarding the original model entirely. Neither of these options is ideal: storing a complete copy is often redundant, especially for minor edits, while losing access to the base model eliminates the ability to encode multiple edits from a shared starting point. Drawing inspiration from recent advances

in parameter-efficient fine-tuning, we address this challenge by leveraging **low-rank adaptations** applied to neural fields.

A LoRA is a rank-constrained additive update to the weight matrices of a neural network. To define this update, recall that an MLP with $h + 1$ layers can be written in the following form:

$$\text{MLP}_\theta(x) = W_h \sigma(W_{h-1} \sigma(W_{h-2} \sigma(\dots (W_1 \sigma(W_0 x)) \dots))), \quad (1)$$

where the matrices W_i contain weights of the neural network (and the bias terms implicitly) and $\sigma(\cdot)$ is an activation. θ contains the elements of the matrices W_i .

Let $W_i \in \mathbb{R}^{d_i^{\text{out}} \times d_i^{\text{in}}}$ be one of the weight matrices in $\{W_0, \dots, W_h\}$ of a pre-trained network, which performs a linear transformation from $\mathbb{R}^{d_i^{\text{in}}}$ to $\mathbb{R}^{d_i^{\text{out}}}$. Rather than fine-tuning W_i directly, the network is fine-tuned by updating $W_i \mapsto W_i + \Delta W_i$, where W_i remains fixed and its adapter ΔW_i satisfies $\text{rank}(\Delta W_i) < \min\{d_i^{\text{in}}, d_i^{\text{out}}\}$.

In particular, following Hu et al. [2022], we factorize

$$\Delta W_i := B_i A_i, \quad (2)$$

where $A_i \in \mathbb{R}^{r \times d_i^{\text{in}}}$, $B_i \in \mathbb{R}^{d_i^{\text{out}} \times r}$, and r is an adjustable parameter. By construction, the rank of the weight update ΔW_i is at most r .

While prior methods predominantly apply LoRA to large foundation models trained on extensive datasets, *we apply LoRA directly to the weights of a neural field to encode edits to the field compactly*. That is, given a neural field f_θ representing a graphics instance \mathcal{D} as well as an edited version \mathcal{D}' , we encode the change from \mathcal{D} to \mathcal{D}' as a LoRA applied to f_θ .

By encoding edits to a neural field as LoRAs, we inherit many of the advantages LoRAs offer in their original context of LLMs. Since LoRAs generalize full fine-tuning (by setting $r = \min\{d_i^{\text{in}}, d_i^{\text{out}}\}$), they enable finer control over the tradeoff between memory footprint and the expressiveness of the network update. For a pre-trained weight matrix $W_0 \in \mathbb{R}^{d_0^{\text{out}} \times d_0^{\text{in}}}$, a rank- r LoRA requires only $r(d_0^{\text{in}} + d_0^{\text{out}})$ parameters, which is significantly fewer than the $d_0^{\text{out}} \times d_0^{\text{in}}$ parameters needed for full fine-tuning, especially when $r \ll d_0^{\text{in}} d_0^{\text{out}} / (d_0^{\text{in}} + d_0^{\text{out}})$.

In this paper, we focus on minor edits, where the information contained in the pre-trained neural field remains relevant. As pointed out in the motivating experiment (§1), LoRAs are a natural fit under this assumption, as they are designed to capture incremental changes to the pre-trained network. Furthermore, as edits are translated into weight updates for a neural field, downstream tasks can be performed by directly querying the LoRA-updated neural field without reference to the original data \mathcal{D} , \mathcal{D}' . We also empirically explore the relationship between the magnitude of the edit between \mathcal{D} , \mathcal{D}' and the performance of LoRAs (§7.4).

5 Encoding Visual Data Variations with LoRA

We explore four graphics applications where our LoRA-based representation can capture changes. For each one, using LoRA to adapt a neural field involves defining a minimization problem with respect to LoRA parameters whose general form is

$$\min_{\{A_i\}_{i=0}^h, \{B_i\}_{i=0}^h} \mathcal{J}(f_{\theta+\text{LoRA}}, \mathcal{D}, \mathcal{D}'), \quad (3)$$

where \mathcal{J} is an application-specific objective functional and $f_{\theta+\text{LoRA}}$ denotes f_θ with the pre-trained parameters $\theta = (W_0, \dots, W_h)$ frozen

and a trainable LoRA update $((A_0, B_0), \dots, (A_h, B_h))$ applied to every weight matrix. In the following subsections, we describe a few possible realizations of \mathcal{J} , including loss functions for regression and energy functionals.

5.1 Image Variations

We represent changes to an input image $\mathcal{D} \in \mathbb{R}^{H \times W \times 3}$ as updates to a base MLP f_θ that maps (sub-)pixel locations to RGB values. To encode the change, we optimize for LoRA parameters following problem (3) by defining

$$\mathcal{J}(f_{\theta+\text{LoRA}}, \mathcal{D}') := \mathbb{E}_{x \sim \text{unif}(\mathcal{X})} [\mathcal{L}(f_{\theta+\text{LoRA}}(x), \mathcal{D}'_x)] \quad (4)$$

where \mathcal{L} is the loss function used to obtain the base model f_θ , \mathcal{X} is a dense set of 2D point samples in the domain of the image, and \mathcal{D}'_x denotes the target field value sampled at $x \in \mathcal{X}$ evaluated using \mathcal{D}' . We use the relative L2 loss for \mathcal{L} .

5.2 Geometric Deformations

Many geometry processing tasks involve small changes that must be stored or transmitted efficiently, e.g., consecutive frames of animated surface or local edits from smoothing [Desbrun et al. 1999] and stylization [Liu and Jacobson 2019]. Here, we represent an input surface \mathcal{D} implicitly as a level set of a neural SDF [Park et al. 2019] f_θ . Surface edits are generated using a modeling tool via, e.g., cage-based or ARAP deformations [Sorkine and Alexa 2007] applied to a meshed version of \mathcal{D} .

Here we define the objective \mathcal{J} similarly to equation (4), where \mathcal{D}'_x now represents SDF values at 3D point samples x instead of RGB colors. Following Müller et al. [2022], our reconstruction loss \mathcal{L} for both base model training and LoRA fine-tuning is the mean average percentage error (MAPE), defined as $\frac{|\text{prediction} - \text{target}|}{|\text{target}| + 0.01}$.

5.3 Energy Minimization

Many visual computing tasks (e.g., smoothing, deformation, or denoising) are framed as energy minimization problems [Chambolle et al. 2010; Crane et al. 2013; Sorkine and Alexa 2007; Taubin 2012]. These tasks modify data by seeking critical points of energy functionals via numerical optimization. Recent work extends this paradigm to neural fields [Marschner et al. 2023; Xu et al. 2022], and we show that LoRA remains compatible.

In this setting, \mathcal{D}' is unknown but characterized as a solution to an energy minimization problem. A general formulation of the objective functional in problem (3) is

$$\mathcal{J}(f_{\theta+\text{LoRA}}, \mathcal{D}) := \mathbb{E}_{x \sim \text{unif}(\mathcal{X})} [\mathcal{L}(f_{\theta+\text{LoRA}}(x), \mathcal{D}_x) + \lambda E(f_{\theta+\text{LoRA}}, x)] \quad (5)$$

where E is a user-defined energy functional, \mathcal{L} is a data fidelity loss encouraging similarity to the original data \mathcal{D} , and $\lambda \in \mathbb{R}_{>0}$ controls the relative importance of the energy and data fidelity terms.

5.4 Encoding Sequential Changes

Whereas the previous applications focus on small edits to a single instance, real-world data often exhibits large or sequential variations, such as temporal changes in videos or animated character motion. To explore this setting, we decompose large variations into a *sequence* of smaller frames and encode each using LoRA.

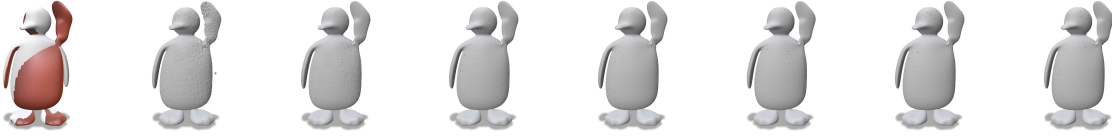
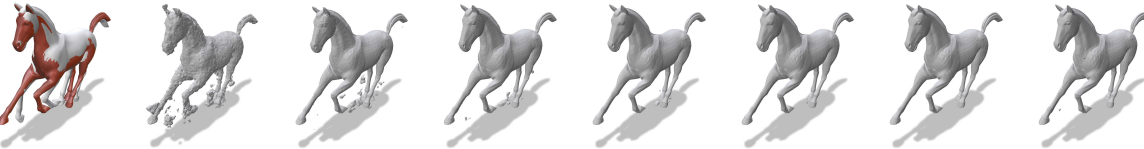

Shape # Params % Params	Input/Target	$r = 1$	$r = 4$	$r = 8$	$r = 16$	$r = 32$	$r = 64$	FT
Penguin	IoU	0.990	0.994	0.996	0.997	0.998	0.998	0.997
								
Horse	IoU	0.922	0.984	0.993	0.996	0.997	0.998	0.998
								
Armadillo	IoU	0.870	0.965	0.976	0.989	0.992	0.992	0.997
								

Fig. 4. Comparison of LoRA-based SDF reconstruction quality (IoU) using increasing rank r against full fine-tuning (FT) for encoding surface deformations. The number of fine-tuning parameters as a percentage of the base model size is shown in the top row.

In doing so, two strategies naturally emerge: (1) train an *independent* LoRA for each frame, adapting a shared base model as in §5.1; or (2) apply LoRA updates *sequentially*, where each update builds on its predecessor. The latter tests our method’s ability to handle long sequences while controlling accumulated error. We evaluate both approaches and describe the sequential version below.

We treat videos and character animations as temporal sequences of static variations, extending the setups in §5.1 and §5.2. To model these frame-to-frame changes, we optimize for LoRA parameters solving problem (3).

In more detail, given a sequence of n frames, we first overfit a base network $f_{\theta,1}$ to frame 1. Then, for each subsequent frame $i \in \{2, \dots, n\}$, we train a LoRA to capture the update from the preceding frame. After applying the LoRA to obtain $f_{\theta,i}$, we freeze its parameters and repeat the process for the next frame. Each LoRA induces a rank- r update, so frame k corresponds to a rank- $r(k-1)$ update to the original base model.

REMARK. *Our proposed pipeline for processing frames sequentially simply optimizes LoRAs one-at-a-time. This algorithm has identical efficiency per frame as the static setting in §5.1 and §5.2. We emphasize that this experiment mainly serves as a stress test of our approach for temporal data.*

6 Implementation Details

Architecture. In all experiments, we use a standard MLP as our base model f_{θ} with a frequency encoding (3) and ReLU activations on the hidden layers. We use 4, 5, and 6 hidden layers for SDF, image, and video, respectively. All hidden layers have width 256.

For the frequency encoding, we use $L = 6$ for SDF experiments and $L = 10$ elsewhere. In practice, one could select base model hyperparameters according to the complexity of the input data. Crucially, the maximum rank hyperparameter r controls the size of the low-rank adapters, and we investigate the impact of the choice of r in §7.3.

Initialization. Following Hayou et al. [2024], we initialize each A_i matrix of our LoRAs using a normal distribution $\mathcal{N}(0, 1/d_i^{in})$ where d_i^{in} is the input dimension of the corresponding base weight $W_i \in \mathbb{R}^{d_i^{out} \times d_i^{in}}$; every B_i matrix is initialized to 0. The update $\Delta W_i = B_i A_i$ is scaled by $1/r_i$ where r_i is the maximum rank of the current adapter.

Setup. We implement our base neural field and LoRA updates in PyTorch. We conduct our experiments on a NVIDIA RTX 3090 GPU, with 24 GB of memory and 1395 MHz clock frequency. We compute SDF samples from meshes using the PySDF Python library [Yu 2023]. We train and fine-tune using the Adam algorithm [Kingma and Ba 2014]. We observed reasonably fast convergence with a learning rate of 10^{-4} for the base neural field f_{θ} . For fair comparison between LoRA and full fine-tuning, we empirically searched for the largest learning rate such that the loss does not diverge: 5×10^{-3} for LoRA and 10^{-4} for full fine-tuning. An improvement-based convergence threshold is used to terminate fine-tuning, and a maximum step budget (3×10^4) is set across all experiments. We rescale coordinates to fit in $[-1, 1]^n$.

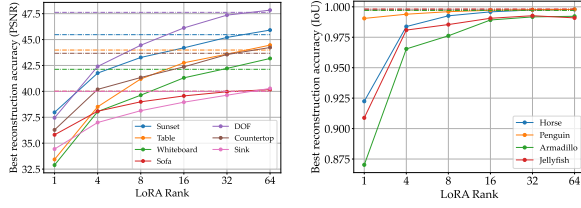


Fig. 5. Image (left) and SDF (right) reconstruction quality of LoRA vs. full-finetuning for image variations and surface deformations, respectively. Dotted line denotes full fine-tuning. See Figure 14 and Figure 4 for the corresponding reconstructions.

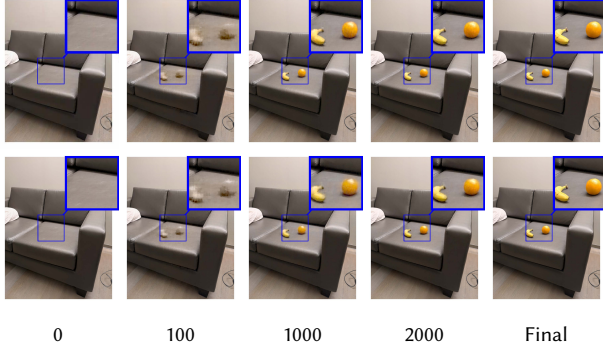


Fig. 6. Intermediate image reconstructions using LoRA (top) and full fine-tuning (bottom). Each column corresponds to a training step. LoRA reconstructions mirror full fine-tuning at convergence and throughout training.

7 Results

Here, we discuss the results of each application presented in §5, comparing the performance of encoding variations using LoRA against full fine-tuning of base neural field f_θ . We also conduct experiments investigating the impact of the LoRA rank hyperparameter (§7.3), the relationship between rank, and the magnitude of variation between \mathcal{D} , \mathcal{D}' (§7.4). Finally, we compare against post hoc low-rank factorization (§7.7) and a network overfitting baseline under a fixed parameter count (§7.8).

Metrics. For surface fitting, we evaluate the zero level set of LoRA-augmented neural SDFs against the target surface \mathcal{D}' using intersection-over-union (IoU), computed using 134 million points sampled uniformly in the bounding box, as in Müller et al. [2022]. IoU ranges from 0 (no overlap) to 1 (perfect match). For images and videos, we report peak signal-to-noise ratio (PSNR) and mean squared error (MSE) against the reference frames.

7.1 Image Variations

Figures 3 and 14 present results on eight image pairs \mathcal{D} , \mathcal{D}' exhibiting diverse variations, including object insertions/removals, lighting changes, temporal changes, depth-of-field adjustments, and post-processing filters. Our LoRA-based representation achieves PSNR values comparable to full fine-tuning—while using 7–8× fewer

parameters. Visually, LoRA reconstructions are nearly indistinguishable from fine-tuned ones (Figure 14) even under challenging edits like the inserted marker strokes in Figure 3. LoRA faithfully reconstructs all tested variations, with only minor degradation for post-processing effects (e.g., stylized filters) which globally alter high-frequency detail in \mathcal{D} .

Additionally, LoRA preserves unedited regions of \mathcal{D} during training, similar to full fine-tuning, and produces competitive intermediate results after only a few iterations (Figure 6). This suggests that the low-rank constraint imposed by LoRA does not adversely affect the training trajectory relative to full fine-tuning, despite allowing a higher stable learning rate.

7.2 Geometric Deformations

Deformations in this experiment are generated by applying skeleton-based transformations to \mathcal{D} . Figure 4 shows that LoRA and full fine-tuning reconstructions differ in IoU by under 0.02 at the default rank ($r = 16$). Visually, both methods preserve fine geometric features—e.g., the ridges on the armadillo—and are nearly indistinguishable. LoRA achieves this while using 85–90% fewer parameters than full fine-tuning. When present, error typically appears as high-frequency noise in the isosurface reconstruction. As with image variations, LoRA’s intermediate reconstructions closely track those of full fine-tuning: artifacts resolve at a similar rate, concentrate in deformed regions, and are minimal in unmodified areas (see Supplemental Material). These results suggest that LoRA can significantly compress neural SDF updates while maintaining stable and predictable training dynamics.

7.3 Impact of LoRA Rank

We train LoRAs with varying ranks ($r = 1, 4, 8, 16, 32, 64$) for images and SDFs to examine the tradeoff between LoRA size and update capacity. As shown in Figure 5, reconstruction quality increases monotonically with r , and ranks $r \geq 16$ consistently match full fine-tuning for both modalities. Beyond $r = 16$ (i.e., > 12% of full fine-tuning parameters), quality continues to improve gradually. At $r = 64$, LoRA slightly outperforms full fine-tuning for images and closely approaches it for SDFs (within 0.003 IoU on average).

Performance degrades gracefully for very small r : noise artifacts grow as expressivity decreases, but many variations remain recognizable even with $r = 1$, a 99% parameter reduction (see Figures 14 and 4). This aligns with our motivating experiment (Figure 2) which revealed a rank threshold below which low-rank factorizations struggle to approximate the full update. When error is visible, it is spatially localized to regions with the largest edits and minimal elsewhere (see Figure 3, right inset; Figure 4, $r = 1, 4$). Overall, LoRA offers a predictable and controllable tradeoff between parameter efficiency and reconstruction fidelity.

7.4 Effect of Variation Magnitude

We investigate the relationship between the magnitude of the variation between \mathcal{D} , \mathcal{D}' and the reconstruction quality using LoRA compared to full fine-tuning.

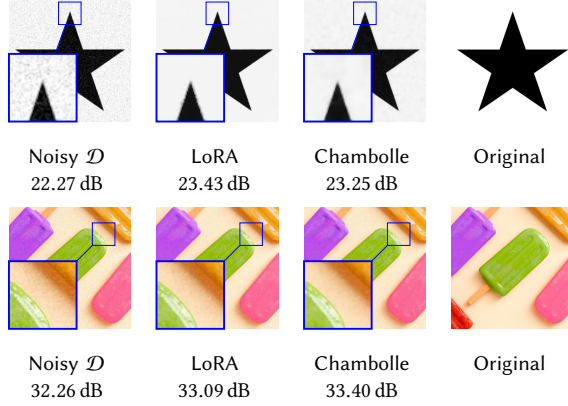


Fig. 7. Total Variation image denoising. Noisy input image regressed by f_θ (left), LoRA TV energy minimization output (center left), Chambolle’s projection algorithm applied to the noisy image (center right), and the original image. PSNR against the original noise-free image is shown. Image by Edy HG.

For images, we controllably edit \mathcal{D} in two ways. Firstly, we apply low-frequency Gaussian noise to the RGB values of \mathcal{D} (by computing per-pixel noise $\Delta x \in \mathbb{R}^{H \times W \times 3}$ where $\Delta x_{ijc} \sim \mathcal{N}(0, \sigma^2)$), applying a low-pass filter to Δx , scaling by $k \geq 1$, and setting $x' := x + k\Delta x$ to obtain \mathcal{D}' . The variation magnitude is controlled by the noise magnitude k . Secondly, we experiment with \mathcal{D}' obtained from applying non-linear distortion filters to \mathcal{D} in image processing software; here, the magnitude is controlled by the software-defined distortion intensity parameter. Figure 12 suggests that LoRA is most competitive with full fine-tuning when the variation is minor. The error gap between successive LoRA ranks and full fine-tuning grows with the difference between \mathcal{D} , \mathcal{D}' . For significant variations where f_θ no longer provides a meaningful initialization for fine-tuning, the LoRAs ineffectively adapt the base model. This is unsurprising, as in practice LoRAs are almost universally applied to capture *small* distributional shifts.

For geometry, we take \mathcal{D} to be a source mesh and take intermediate meshes from a physical simulation [Mattos Da Silva et al. 2025] of \mathcal{D} to use as \mathcal{D}' . As the mesh continually deforms away from its rest state, we use the simulation time step as a proxy for the variation magnitude. Figure 13 reveals the same pattern previously observed with images.

7.5 Energy Minimization

We experiment with the *Total Variation* energy defined as $E_{TV}(f, x) := \|\nabla_x f(x)\|_2$, where $\nabla_x f(x)$ denotes the spatial gradient of an input function f . Solving problem (5) with E_{TV} is a neural field adaptation of the well-studied Total Variation denoising (TVD) problem [Rudin et al. 1992]. TVD is known to remove noise while preserving sharp edges in the underlying signal. Unlike conventional low-pass filters, the result of TVD is obtained through numerical optimization.

In this setting, f_θ parameterizes a noisy input image (obtained by adding Gaussian noise), and $f_{\theta+\text{LoRA}}$ seeks to denoise. We estimate the gradient via a finite difference. We compare our denoised result

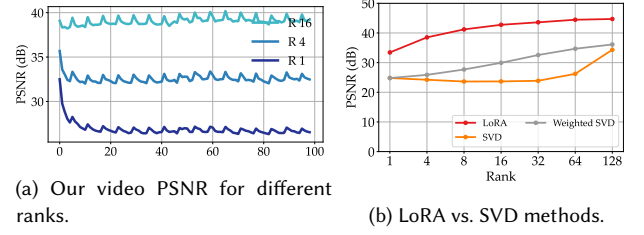


Fig. 8. Comparison of our neural field update methods across different ranks. (a) Per-frame video reconstruction quality (PSNR) for different LoRA ranks ($R = 1, 4, 16$) showing stable performance over 100 frames. (b) Reconstruction quality comparison between our LoRA method, truncated SVD, and weighted SVD across varying ranks. LoRA consistently outperforms both SVD baselines, with the performance gap increasing at higher ranks.

with that of applying Chambolle’s projection algorithm—a standard approach for TVD on images—applied to the output of f_θ . Figure 7 shows that minimizing E_{TV} over LoRA parameters yields an edge-preserving denoising effect, as desired.

7.6 Sequential LoRAs

We apply the sequential LoRA training procedure outlined in §5.4 to encode real 1080p video footage (Figure 11) and an animation (see Supplemental Material) with 100 and 130 frames, respectively. Even with basic sequential optimization, our method is able to encode long sequences of frame-to-frame changes with no apparent long-term error accumulation. Figure 8a shows per-frame reconstruction accuracy for the video footage using sequential LoRAs with varying ranks. While there is local fluctuation between small subsequences of frames, the PSNR globally remains within 39.2 ± 1 dB for the captured video ($r = 16$) and 37.1 ± 1.8 dB for the animation. Even at very low ranks ($r \leq 4$), error drift is minimal past the initial frames. See the Supplemental Material for video reconstructions.

We also evaluate the parallel encoding strategy described in §5.4 on animated surfaces, where each frame \mathcal{D}' is obtained from physical simulation and is *independently* encoded as a LoRA update to the rest-state model ($t = 0$). This setup is trivially parallelizable, taking no more time than training a single LoRA. Figure 13 shows that this approach performs well for a small number of frames (≤ 5) across all ranks $r \geq 4$ but struggles with $r = 1$, especially at larger time steps. This behavior is consistent with the variation magnitude observations in §7.4.

7.7 Post-hoc Low-Rank Factorization Baseline

To assess parameter efficiency, we compare against low-rank factorization of the weight difference matrices performed *after* full fine-tuning as a baseline. As mentioned in the motivating experiment in §1, a low-rank factorization of each layer’s weight difference $\Delta W := W_{\text{fine-tuned}} - W_{\text{base}}$ approximates the true difference with relatively low error (with respect to a matrix norm). We now compare the output reconstruction quality using LoRA against (1) the rank- r truncated singular value decomposition (SVD) of ΔW , and (2) a weighted variant of truncated SVD that accounts for each network layer’s input distribution (see Supplemental Materials).

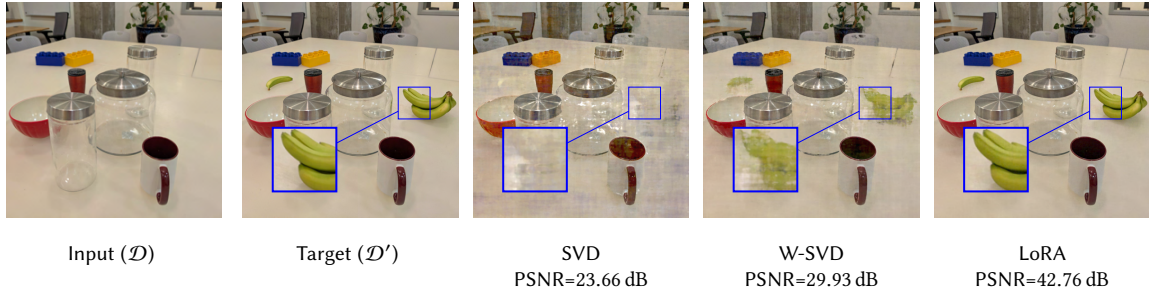


Fig. 9. Comparison of image reconstructions using our LoRA vs. the truncated singular value decomposition of the full network weight differences (SVD) and a weighted variant of truncated SVD (W-SVD). All approaches use $r = 16$.



Fig. 10. We compare reconstructions of image variations using LoRA vs. with a small MLP containing the same number of parameters (46.9k). From left to right: input image \mathcal{D} , target variation \mathcal{D}' , reconstruction from a small MLP trained from scratch, and the result from our LoRA method. The small MLP struggles to capture as many fine details as LoRA (PSNR: 26.3 dB vs. 28.2 dB respectively). Input photos by Eirik Solheim.

Figure 8b shows that LoRA image reconstruction PSNR consistently exceeds both SVD and weighted SVD by 10 dB across all ranks. In Figure 9, we show an example where vanilla SVD struggles to encode the desired change, while weighted SVD only captures a blurry change. Furthermore, both SVD approaches produce significant global artifacts which—unlike LoRA—are pronounced in unmodified regions of the target image. Although truncated SVD provides the theoretically optimal low-rank factorization for each individual layer’s ΔW (w.r.t. Frobenius norm), this experiment suggests that the online and reconstruction-loss-aware factorization using LoRA significantly benefits the reconstruction accuracy of the neural field’s final output.

7.8 Fixed-parameter-count Baseline

To determine whether the low-rank constraint on the weight updates encourages them to encode a minor *offset* from \mathcal{D} rather than simply parameterizing the *entire* edited instance \mathcal{D}' , we perform a fixed-parameter-count comparison. We compare the reconstruction quality of \mathcal{D}' using $f_{\theta+\text{LoRA}}$ against that using a new neural field $f_{\theta'}$ trained from scratch with the same number of parameters as the LoRA, i.e., $\text{size}(\text{LoRA}) = \text{size}(\theta')$. $f_{\theta'}$ has the same architecture as f_{θ} but a uniformly lower hidden layer size chosen so that $f_{\theta'}$ has parameter count as close to $\text{size}(\text{LoRA})$ as possible. We carry out this comparison on a difficult input image which the base model can barely regress. Figure 10 shows a decrease in reconstruction quality for both our LoRAs and the small MLP baseline. However, with the same number of parameters, our LoRAs visibly preserve details that the baseline cannot resolve, outperforming the baseline by 1.9 dB.

8 Conclusion

Redundancy is pervasive in graphics and has long been leveraged for efficient representations across different signal modalities—such as in video compression and mesh simplification—where redundancy can be understood in lower-dimensional domains. Neural fields, however, pose a unique challenge: they lift low-dimensional signals into high-dimensional representations, making it less obvious how to think about redundancy. In this work, we demonstrate that low-rank adaptation offers a principled and effective lens for understanding and leveraging redundancy in neural fields.

We show LoRA updates enable versatile neural field editing for images and surfaces, plus extensions to energy minimization and dynamic data. Our method provides fine-grained control over the expressivity-storage trade-off. We empirically demonstrate this trade-off is predictable where reconstruction quality degrades gracefully at low ranks and high variations, with error artifacts appearing in expected output regions.

Our method’s training speed is limited by the base neural field’s size and architecture. Since LoRA optimization requires backpropagating through the entire base model each iteration, with the backward pass dominating tuning time, our unoptimized implementation runs no faster per iteration than full fine-tuning despite matching intermediate outputs. Both methods achieve adequate results in under 5 minutes but need 20-30 minutes for full convergence. Thus, exploring more time-efficient LoRA updates is a valuable direction for future work.

Acknowledgments

The MIT Geometric Data Processing Group acknowledges the generous support of Army Research Office grant W911NF2110293, of National Science Foundation grants IIS2335492 and OAC2403239, from the CSAIL Future of Data and FinTechAI programs, from the MIT-IBM Watson AI Laboratory, from the Wistron Corporation, from the MIT Generative AI Impact Consortium, from the Toyota-CSAIL Joint Research Center, and from Schmidt Sciences. We thank Leticia Mattos da Silva for providing the Jellyfish animation, Silvia Sellán for assistance with manuscript preparation, and Ana Dodik for the image of Bella the dog and for valuable discussions. Big Buck Bunny (2008 Blender Foundation) is licensed under the Creative Commons Attribution 3.0 (CC BY 3.0) license.

References

- Andy Beach and Aaron Owen. 2018. *Video Compression Handbook* (2nd ed.). Peachpit Press.
- Antonin Chambolle, Vicent Caselles, Daniel Cremers, Matteo Novaga, and Thomas Pock. 2010. An introduction to total variation for image analysis. *Theoretical foundations and numerical methods for sparse recovery* 9, 263–340 (2010), 227. <http://cvgmt.sns.it/paper/2007/>
- Anpei Chen, Zexiang Xu, Andreas Geiger, Jingyi Yu, and Hao Su. 2022. TensoRF: Tensorial Radiance Fields. In *European Conference on Computer Vision* (Tel Aviv, Israel). Springer-Verlag, 333–350. doi:10.1007/978-3-031-19824-3_20
- Hao Chen, Bo He, Hanyu Wang, Yixuan Ren, Ser-Nam Lim, and Abhinav Shrivastava. 2021. NeRV: Neural representations for videos. In *Proceedings of the 35th International Conference on Neural Information Processing Systems (NIPS '21, Vol. 34)*. Curran Associates Inc., Red Hook, NY, USA, Article 1649, 12 pages.
- Pei-Ze Chiang, Meng-Shiun Hsai, Hung-Yu Tseng, Wei-Sheng Lai, and Wei-Chen Chiu. 2022. Stylizing 3D scene via implicit representation and hypernetwork. In *2022 IEEE/CVF Winter Conference on Applications of Computer Vision (WACV)*. IEEE Computer Society, Los Alamitos, CA, USA, 215–224. doi:10.1109/WACV51458.2022.00029
- Robert L. Cook. 1984. Shade trees. *SIGGRAPH Comput. Graph.* 18, 3 (July 1984), 223–231. doi:10.1145/964965.808602
- Keenan Crane, Ulrich Pinkall, and Peter Schröder. 2013. Robust fairing via conformal curvature flow. *ACM Transactions on Graphics (TOG)* 32, 4, Article 61 (July 2013), 10 pages. doi:10.1145/2461912.2461986
- Rishit Dagli, Atsuhiko Hibi, Rahul G. Krishnan, and Pascal N. Tyrrell. 2024. NeRF-US: Removing Ultrasound Imaging Artifacts from Neural Radiance Fields in the Wild. (Aug. 2024). arXiv:2408.10258 [cs.CV] <https://arxiv.org/abs/2408.10258>
- Thomas Davies, Derek Nowrouzezahrai, and Alec Jacobson. 2021. Overfit Neural Networks as a Compact Shape Representation. (Jan. 2021). arXiv:2009.09808 [cs.GR] <https://arxiv.org/abs/2009.09808>
- Mathieu Desbrun, Mark Meyer, Peter Schröder, and Alan H. Barr. 1999. Implicit Fairing of Irregular Meshes Using Diffusion and Curvature Flow. In *Proceedings of the 26th Annual Conference on Computer Graphics and Interactive Techniques (SIGGRAPH '99)*. ACM Press/Addison-Wesley Publishing Co., USA, 317–324. doi:10.1145/311535.311576
- Zekun Hao, Hadar Averbuch-Elor, Noah Snavely, and Serge Belongie. 2020. DualSDF: Semantic Shape Manipulation using a Two-Level Representation. In *Proceedings of the IEEE/CVF Conference on Computer Vision and Pattern Recognition (CVPR)*. 7631–7641. <https://doi.ieeecomputersociety.org/10.1109/CVPR42600.2020.00765>
- Soufiane Hayou, Nikhil Ghosh, and Bin Yu. 2024. The Impact of Initialization on LoRA Finetuning Dynamics. *ArXiv abs/2406.08447* (2024). <https://api.semanticscholar.org/CorpusID:270391476>
- Edward Hu, Yelong Shen, Phillip Wallis, Zeyuan Allen-Zhu, Yuanzhi Li, Shean Wang, Lu Wang, and Weizhu Chen. 2022. LoRA: Low-Rank Adaptation of Large Language Models. In *International Conference on Learning Representations (ICLR 2022)*. <https://openreview.net/forum?id=nZeVKeeFYf9>
- Gyeongjin Kang, Younggeun Lee, Seungjun Oh, and Eunbyung Park. 2025. CodecNeRF: Toward Fast Encoding and Decoding, Compact, and High-quality Novel-view Synthesis. In *Proceedings of the AAAI Conference on Artificial Intelligence*, Vol. 39, 4203–4211.
- Taehwan Kim and Tülay Adalı. 2003. Approximation by Fully Complex Multi-layer Perceptrons. *Neural computation* 15, 7 (July 2003), 1641–1666. doi:10.1162/089976603321891846
- Diederik P. Kingma and Jimmy Ba. 2014. Adam: A Method for Stochastic Optimization. *arXiv preprint arXiv:1412.6980* (2014).
- Jae-Hyeok Lee and Dae-Shik Kim. 2023. ICE-NeRF: Interactive Color Editing of NeRFs via Decomposition-Aware Weight Optimization. In *2023 IEEE/CVF International Conference on Computer Vision (ICCV)*. 3468–3478. doi:10.1109/ICCV51070.2023.00323
- Chenxi Liu, Towaki Takikawa, and Alec Jacobson. 2024. A LoRA is Worth a Thousand Pictures. arXiv:2412.12048 [cs.CV] <https://arxiv.org/abs/2412.12048>
- Hsueh-Ti Derek Liu and Alec Jacobson. 2019. Cubic stylization. *ACM Transactions on Graphics (TOG)* 38, 6, Article 197 (Nov. 2019), 10 pages. doi:10.1145/3355089.3356495
- Steven Liu, Xiuming Zhang, Zhoutong Zhang, Richard Zhang, Jun-Yan Zhu, and Bryan Russell. 2021. Editing Conditional Radiance Fields. In *2021 IEEE/CVF International Conference on Computer Vision (ICCV)*. IEEE Computer Society, Los Alamitos, CA, USA, 5773–5783. doi:10.1109/ICCV48922.2021.00572
- Ziqi Lu, Heng Yang, Danfei Xu, Boyi Li, Boris Ivanovic, Marco Pavone, and Yue Wang. 2024. LoRA3D: Low-Rank Self-Calibration of 3D Geometric Foundation Models. (Dec. 2024). arXiv:2412.07746 [cs.CV] <https://arxiv.org/abs/2412.07746>
- Lorenzo Luzi, Daniel LeJeune, Ali Siahkoobi, Sina Alemohammad, Vishwanath Saragadam, Hossein Babaei, Naiming Liu, Zichao Wang, and Richard G. Baraniuk. 2024. TITAN: Bringing the Deep Image Prior to Implicit Representations. In *ICASSP 2024 - 2024 IEEE International Conference on Acoustics, Speech and Signal Processing (ICASSP)*. 6165–6169. doi:10.1109/ICASSP48485.2024.10446136
- Zoë Marschner, Silvia Sellán, Hsueh-Ti Derek Liu, and Alec Jacobson. 2023. Constructive Solid Geometry on Neural Signed Distance Fields (SA '23). Association for Computing Machinery, New York, NY, USA, Article 121, 12 pages. doi:10.1145/3610548.3618170
- Julien N. P. Martel, David B. Lindell, Connor Z. Lin, Eric R. Chan, Marco Monteiro, and Gordon Wetzstein. 2021. ACORN: Adaptive Coordinate Networks for Neural Scene Representation. *ACM Transactions on Graphics (TOG)* 40, 4, Article 58 (July 2021), 13 pages. doi:10.1145/3450626.3459785
- Leticia Mattos Da Silva, Silvia Sellán, Natalia Pacheco-Tallaj, and Justin Solomon. 2025. Variational Elastodynamic Simulation. In *Proceedings of the Special Interest Group on Computer Graphics and Interactive Techniques Conference Conference Papers (SIGGRAPH Conference Papers '25)*. Association for Computing Machinery, New York, NY, USA, Article 76, 11 pages. doi:10.1145/3721238.3730726
- Alessio Mazzucchelli, Adrian Garcia-Garcia, Elena Garces, Fernando Rivas-Manzanique, Francesc Moreno-Noguer, and Adrian Penate-Sanchez. 2024. IReNe: Instant Recoloring of Neural Radiance Fields. In *2024 IEEE/CVF Conference on Computer Vision and Pattern Recognition (CVPR)*. 5937–5946. doi:10.1109/CVPR52733.2024.00567
- Ishit Mehta, Manmohan Chandraker, and Ravi Ramamoorthi. 2022. A Level Set Theory for Neural Implicit Evolution Under Explicit Flows. In *European Conference on Computer Vision* (Tel Aviv, Israel). Springer-Verlag, 711–729. doi:10.1007/978-3-031-20086-1_41
- Lars Mescheder, Michael Oechsle, Michael Niemeyer, Sebastian Nowozin, and Andreas Geiger. 2019. Occupancy Networks: Learning 3D Reconstruction in Function Space. In *Proceedings of the IEEE/CVF conference on computer vision and pattern recognition*. 4455–4465. doi:10.1109/CVPR.2019.00459
- Ben Mildenhall, Pratul P. Srinivasan, Matthew Tancik, Jonathan T. Barron, Ravi Ramamoorthi, and Ren Ng. 2021. NeRF: Representing Scenes as Neural Radiance Fields for View Synthesis. *Commun. ACM* 65, 1 (Dec. 2021), 99–106. doi:10.1145/3503250
- Vismay Modi, Nicholas Sharp, Or Perel, Shinjiro Sueda, and David I. W. Levin. 2024. Simplicits: Mesh-Free, Geometry-Agnostic Elastic Simulation. *ACM Transactions on Graphics (TOG)* 43, 4, Article 117 (July 2024), 11 pages. doi:10.1145/3658184
- Thomas Müller, Alex Evans, Christoph Schied, and Alexander Keller. 2022. Instant Neural Graphics Primitives with a Multiresolution Hash Encoding. *ACM Transactions on Graphics (TOG)* 41, 4, Article 102 (July 2022), 15 pages. doi:10.1145/3528223.3530127
- Wenqi Ouyang, Yi Dong, Lei Yang, Jianlou Si, and Xingang Pan. 2024. I2VEdit: First-Frame-Guided Video Editing via Image-to-Video Diffusion Models. In *SIGGRAPH Asia 2024 Conference Papers (SA '24)*. Association for Computing Machinery, New York, NY, USA, Article 95, 11 pages. doi:10.1145/3680528.3687656
- Jeong Joon Park, Peter Florence, Julian Straub, Richard Newcombe, and Steven Lovegrove. 2019. DeepSDF: Learning Continuous Signed Distance Functions for Shape Representation. In *Proceedings of the IEEE/CVF conference on computer vision and pattern recognition*. 165–174. doi:10.1109/CVPR.2019.00025
- Zhangyang Qi, Yunhan Yang, Mengchen Zhang, Long Xing, Xiaoyang Wu, Tong Wu, Dahua Lin, Xihui Liu, Jiaqi Wang, and Hengshuang Zhao. 2024. Tailor3D: Customized 3D Assets Editing and Generation with Dual-Side Images. *arXiv preprint arXiv:2407.06191* (2024).
- M. Raissi, P. Perdikaris, and G.E. Karniadakis. 2019. Physics-informed neural networks: A deep learning framework for solving forward and inverse problems involving nonlinear partial differential equations. *J. Comput. Phys.* 378 (2019), 686–707. doi:10.1016/j.jcp.2018.10.045
- Leonid I. Rudin, Stanley Osher, and Emad Fatemi. 1992. Nonlinear total variation based noise removal algorithms. *Physica D: Nonlinear Phenomena* 60, 1 (1992), 259–268. doi:10.1016/0167-2789(92)90242-F
- Viraj Shah, Nataniel Ruiz, Forrester Cole, Erika Lu, Svetlana Lazebnik, Yuanzhen Li, and Varun Jampani. 2025. ZipLoRA: Any Subject in Any Style by Effectively Merging LoRAs. In *Computer Vision – ECCV 2024*. Aleš Leonardis, Elisa Ricci, Stefan Roth, Olga Russakovsky, Torsten Sattler, and Gül Varol (Eds.). Springer Nature Switzerland, Cham, 422–438. doi:10.1007/978-3-031-73232-4_24
- Nicholas Sharp and Alec Jacobson. 2022. Spelunking the Deep: Guaranteed Queries on General Neural Implicit Surfaces via Range Analysis. *ACM Transactions on Graphics (TOG)* 41, 4, Article 107 (July 2022), 16 pages. doi:10.1145/3528223.3530155
- Vincent Sitzmann, Julien Martel, Alexander Bergman, David Lindell, and Gordon Wetzstein. 2020. Implicit Neural Representations with Periodic Activation Functions. *Advances in Neural Information Processing Systems* 33 (2020), 7462–7473.
- Olga Sorkine and Marc Alexa. 2007. As-Rigid-As-Possible Surface Modeling. In *Proceedings of the Fifth Eurographics Symposium on Geometry Processing* (Barcelona, Spain) (SGP '07). Eurographics Association, Goslar, DEU, 109–116.
- Towaki Takikawa, Joey Litalien, Kangxue Yin, Karsten Kreis, Charles Loop, Derek Nowrouzezahrai, Alec Jacobson, Morgan McGuire, and Sanja Fidler. 2021. Neural Geometric Level of Detail: Real-time Rendering with Implicit 3D Shapes. In *Proceedings of the IEEE/CVF Conference on Computer Vision and Pattern Recognition*. 11353–11362. doi:10.1109/CVPR46437.2021.01120
- Towaki Takikawa, Thomas Müller, Merlin Nimier-David, Alex Evans, Sanja Fidler, Alec Jacobson, and Alexander Keller. 2023a. Compact Neural Graphics Primitives with Learned Hash Probing. In *SIGGRAPH Asia 2023 Conference Papers* (Sydney, NSW, Australia) (SA '23). Association for Computing Machinery, New York, NY, USA, Article 120, 10 pages. doi:10.1145/3610548.3618167
- Towaki Takikawa, Shunsuke Saito, James Tompkin, Vincent Sitzmann, Srinath Sridhar, Or Litany, and Alex Yu. 2023b. Neural Fields for Visual Computing: SIGGRAPH 2023



Fig. 11. We encode a high-resolution video as sequential LoRA updates from an initial frame (see §5.4). Here, we visualize reconstructions of four frames using full fine-tuning (406.1k parameters) vs. LoRA (54.6k parameters) and report the reconstruction accuracy.

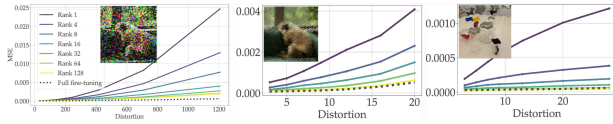


Fig. 12. We synthetically vary images by adding low-frequency Gaussian noise (left), applying a glass style filter (center), and applying a wave-style distortion filter (right). The graphs in the top row show reconstruction error for increasing variation magnitudes across different LoRA ranks and full fine-tuning.

- Course. In *ACM SIGGRAPH 2023 Courses* (Los Angeles, California) (SIGGRAPH '23). Association for Computing Machinery, New York, NY, USA, Article 10, 227 pages. doi:10.1145/3587423.3595477
- Gabriel Taubin. 2012. Introduction to Geometric Processing through Optimization. *IEEE Computer Graphics and Applications* 32, 4 (2012), 88–94. doi:10.1109/MCG.2012.80
- Sheng-Yu Wang, David Bau, and Jun-Yan Zhu. 2022. Rewriting Geometric Rules of a GAN. *ACM Transactions on Graphics (TOG)* 41, 4, Article 73 (July 2022), 16 pages. doi:10.1145/3528223.3530065
- Yifan Wang, Lukas Rahmann, and Olga Sorkine-Hornung. 2021. Geometry-Consistent Neural Shape Representation with Implicit Displacement Fields. *CoRR* abs/2106.05187 (2021). arXiv:2106.05187 <https://arxiv.org/abs/2106.05187>
- Zhengyi Wang, Cheng Lu, Yikai Wang, Fan Bao, Chongxuan Li, Hang Su, and Jun Zhu. 2024. Prolificdreamer: High-fidelity and diverse text-to-3d generation with variational score distillation. *Advances in Neural Information Processing Systems* 36 (2024).
- Dejia Xu, Peihao Wang, Yifan Jiang, Zhiwen Fan, and Zhangyang Wang. 2022. Signal Processing for Implicit Neural Representations. In *Proceedings of the 36th International Conference on Neural Information Processing Systems* (New Orleans, LA, USA) (NIPS '22). Red Hook, NY, USA, Article 975, 15 pages.
- Alex Yu. 2023. PySDF. <https://pyapi.org/project/pysdf/> Accessed: 2024-12-01.
- Rui Zhao, Yuchao Gu, Jay Zhangjie Wu, David Junhao Zhang, Jia-Wei Liu, Weijia Wu, Jussi Keppo, and Mike Zheng Shou. 2024. MotionDirector: Motion Customization of Text-to-Video Diffusion Models. In *European Conference on Computer Vision* (Milan, Italy). Springer-Verlag, Berlin, Heidelberg, 273–290. doi:10.1007/978-3-031-72992-8_16

$r = 1$	$r = 4$	$r = 8$	$r = 16$	$r = 32$	$r = 64$	FT
0.940	0.981	0.985	0.989	0.991	0.992	0.997
0.934	0.978	0.988	0.991	0.992	0.992	0.998
0.909	0.980	0.985	0.991	0.993	0.991	0.998
0.891	0.987	0.988	0.992	0.993	0.993	0.998
0.870	0.979	0.987	0.990	0.992	0.994	0.998
0.796	0.983	0.988	0.989	0.993	0.993	0.998

Fig. 13. Surface reconstructions using LoRAs of varying ranks r vs. full fine-tuning (FT). Each row corresponds to a different target surface \mathcal{D}' obtained at increasing timesteps of a physical simulation of \mathcal{D} [Mattos Da Silva et al. 2025]. IoU is shown. See Figure 4 for the parameter count corresponding to each LoRA rank


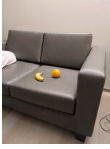
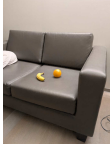


















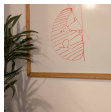






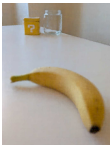








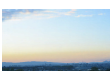
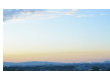
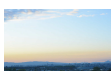
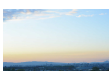
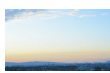


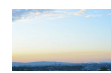


















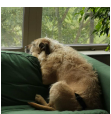

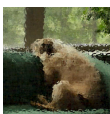
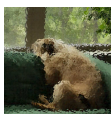
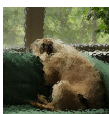
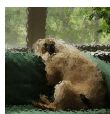
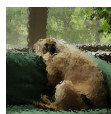
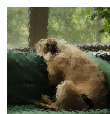
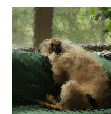
Scene	Input (\mathcal{D})	$r = 1$ 3.1 k 0.9	$r = 4$ 12.4 k 3.6	$r = 8$ 23.8 k 7.0	$r = 16$ 46.7 k 13.7	$r = 32$ 92.4 k 27.1	$r = 64$ 176.7 k 51.9	FT 340.4 k 100	Target (\mathcal{D}')
Sofa	PSNR	35.8 dB	38.1 dB	38.9 dB	39.6 dB	39.9 dB	40.1 dB	40.0 dB	
									
Table	PSNR	33.4 dB	38.5 dB	41.1 dB	42.7 dB	43.5 dB	44.4 dB	43.9 dB	
									
Whiteboard	PSNR	32.8 dB	38.1 dB	39.6 dB	41.3 dB	42.2 dB	43.1 dB	42.1 dB	
									
DOF	PSNR	37.4 dB	42.4 dB	44.45 dB	46.1 dB	47.3 dB	47.8 dB	47.6 dB	
									
Sunset	PSNR	37.9 dB	41.7 dB	43.2 dB	44.2 dB	45.2 dB	45.9 dB	45.4 dB	
									
Countertop	PSNR	36.2 dB	40.2 dB	41.3 dB	42.3 dB	43.5 dB	44.2 dB	43.6 dB	
									
Sink	PSNR	34.4 dB	36.9 dB	38.13 dB	38.9 dB	39.6 dB	40.2 dB	39.9 dB	
									
Glass Filter	PSNR	25.5 dB	28.1 dB	30.2 dB	32.3 dB	34.4 dB	35.7 dB	35.1 dB	
									

Fig. 14. Comparison of LoRA-based image reconstructions using increasing rank r against full fine-tuning (FT) for encoding image variations. The number of fine-tuning parameters as a percentage of the base model size is shown in the top row.